Redshift Evolution of the HII Galaxy L–σ Relation: Gaussian Process Analysis and Cosmological Implications

Jiaze Gao,[1] Yun Chen,[2,3,*] and Lixin Xu[1,†]

[1] *Institute of Theoretical Physics, School of Physics, Dalian University of Technology Dalian 116024, People's Republic of China*

[2] *National Astronomical Observatories, Chinese Academy of Sciences Beijing 100101, China*

[3] *College of Astronomy and Space Sciences, University of Chinese Academy of Sciences Beijing, 100049, China*

(Dated: August 5, 2025)

The utility of HII starburst galaxies (HIIGs) as cosmic standard candles relies on the empirical L–σ relation between the Hβ luminosity (L) and ionized gas velocity dispersion (σ). However, the classic scaling L–σ relation well-calibrated with the low-redshift HIIGs fails to properly describe their high-redshift counterparts. To address this, we try to explore new parameterization of the L–σ relation, which is expected to be valid across all redshifts. Using Gaussian process reconstruction of the Hubble diagram from the Pantheon+ supernovae Ia sample, we compare three modified versions of the L–σ relation against the classic scaling form through Bayesian evidence analysis. Our results identify the logarithmic redshift-dependent correction as the most statistically favored parameterization. This conclusion remains valid when repeating the analysis in the ΛCDM model with cosmological parameters fixed to their Planck 2018 fiducial values, which demonstrates the robustness of our results across different cosmological distance estimation approaches. After accounting for Malmquist bias effects, we still detect redshift evolution in the $L-\sigma$ relation, albeit with reduced statistical significance. Furthermore, we perform cosmological analysis within the ΛCDM model from a joint sample of HIIGs and giant extragalactic HII regions (GEHRs), and yield constraints on H_0 and Ω_m that are approximately one order of magnitude less precise than Planck 2018 results.

I. INTRODUCTION

HIIGs are compact systems typically found in dwarf irregular galaxies undergoing intense bursts of star formation, driven by young super stellar clusters. Their optical spectra exhibit strong emission lines from gas ionized by these massive clusters within the host galaxies [1–9]. A key feature of HIIGs is the empirical correlation between the integrated Hβ luminosity (L(Hβ)) and the ionized gas velocity dispersion (σ). This L–σ relation enables HIIGs to serve as potential standard candles, offering a promising avenue for cosmological studies (e.g., [9–17]). The physical basis of the L–σ relation lies in the scaling of both ionizing photon production ($\propto L$(Hβ)) and gas kinematics ($\propto \sigma$) with the mass of the young stellar cluster [3, 4, 7, 8].

The use of HIIGs as "standard candles" heavily relies on the validity of L–σ relation, and the empirical L–σ relation has been widely discussed over the past few decades [3, 4, 7–9, 18–29]. Notably, Chávez *et al.* [8] compiles a sample of 128 HIIGs spanning a redshift range of $0.02 \lesssim z \lesssim 0.2$, where the integrated H$\beta$ fluxes (i.e., f(Hβ)) are measured from low dispersion wide aperture spectrophotometry, and there is $f(\mathrm{H}\beta) \propto L(\mathrm{H}\beta)$; and the ionized gas velocity dispersions (σ) are measured from the high equivalent widths of their Balmer emission lines with the observations of high S/N high-dispersion spectroscopy. Their findings demonstrate a strong and stable L–σ relation within the selected sample.

While the local scaling L–σ relation, i.e., $\log L(\mathrm{H}\beta) \propto \log \sigma$[1], has been thoroughly characterized, its extrapolation to high-redshift regimes remains uncertain. The well-calibrated low-redshift relation may not necessarily hold for distant HII galaxies [23, 29–33]. Recent work by [29] has discovered redshift evolution in the $L-\sigma$ relation. Their analysis reveals systematic variations in the relation's slope between local ($z < 0.2$) and distant ($z > 0.6$) populations, suggesting evolutionary effects that must be accounted for in cosmological applications.

The analysis of Cao and Ratra [29] simultaneously constrained both the $L-\sigma$ relation parameters and cosmological model, which may introduce potential model-dependent systematics. To avoid cosmological model dependencies inherent in Cao and Ratra [29]'s joint analysis, we reconstruct the Hubble diagram using Gaussian Processes with the Pantheon+ SNe Ia sample [34]. We will then examine whether the redshift evolution of the scaling L–σ relation obtained from Cao and Ratra [29] is valid and reliable. If the redshift evolution is verified to be true, we will explore and compare some possible corrections to the classic scaling L–σ relation. Furthermore, we also assess factors that may introduce systematic biases in our primary findings. This model-independent

* chenyun@bao.ac.cn

† lxxu@dlut.edu.cn

[1] where "log" denotes the logarithm base 10.

calibration framework will enhance the reliability of HIIGs as cosmological probes, particularly for high-redshift applications where traditional standard candles become observationally challenging.

The rest of the paper is organized as follows. In Section II, we describe the HIIG sample used in this work and employ Gaussian Process regression to reconstruct model-independent distance moduli with Pantheon+ SNe Ia data, which are subsequently applied to calibrate the HIIG measurements. In Section III, we compare and analyze several possible corrections to the classic scaling L–σ relation and perform corresponding cosmological applications. Section IV addresses key systematic uncertainties and their potential impact on our results. We conclude with a synthesis of our findings and their consequences for future HIIG-based cosmology.

II. DATA AND METHODOLOGY

A. HIIGs dataset and empirical L–σ relation

Both GEHRs and HIIGs are compact systems undergoing massive bursts of star formation [2–4, 6, 10, 13]. However, they differ in their host environments: GEHRs are typically found in the outer disks of late-type galaxies, whereas HIIGs reside in dwarf irregular galaxies. Due to their shared origin in intense star-forming activity, GEHRs and HIIGs exhibit nearly identical optical spectra, dominated by strong emission lines from gas ionized by young, massive star clusters. Consequently, both systems follow the $L-\sigma$ relation, though this relation primarily reflects the properties of the young starbursts rather than their host galaxies. Given their spectral and dynamical similarities, GEHRs—being nearby—are often used as calibrators for the more distant HIIGs [3, 4, 10, 13, 15, 18–21].

The data set used in our analysis includes the measurements of 181 HIIGs and 36 GEHRs. The HIIGs sample comprises 107 low-redshift sources ($0.0088 < z < 0.1642$) from [8], and 74 high-redshift sources ($0.6364 < z < 2.5449$) from [9, 14, 16]. Our GEHRs sample originates from Fernández Arenas *et al.* [15] observations, where these GEHRs reside in 13 local ($z \sim 0$) galaxies.

In this work, three steps are used to associate the observations of HIIGs or GEHRs with the cosmological distance, as described below.

(i) In the practical observations, one can obtain the integrated Hβ emission-line flux, $f(\mathrm{H}\beta)$, from wide-aperture low-resolution spectrophotometry, and measure the corresponding emission line velocity dispersion, σ, from high-resolution spectroscopy.

(ii) The luminosity, $L(\mathrm{H}\beta)$, for each HIIG or GEHR can be calculated based on a given L–σ relation, e.g., the **classic scaling L–σ relation**

$$\log L(\mathrm{H}\beta) = \alpha + \beta \log \sigma. \tag{1}$$

(iii) Once obtaining $f(\mathrm{H}\beta)$ and $L(\mathrm{H}\beta)$ from the above steps and also using the definition of luminosity distance, i.e., $L = 4\pi d_{\mathrm{L}}^2 f$, one can further calculate the luminosity distance (d_{L}) for each HIIG or GEHR,

$$d_{\mathrm{L}}^2 = \frac{L(\mathrm{H}\beta)}{4\pi f(\mathrm{H}\beta)}. \tag{2}$$

And then, the distance modulus $\mu(z)$ can be obtained as follows,

$$\mu(z) = 5 \log d_{\mathrm{L}}(z) + 25, \tag{3}$$

where d_{L} has units of Mpc.

B. Reconstructing the Hubble diagram with SNe Ia data by using Gaussian Process

As mentioned previously, to avoid the dependence on the cosmological model, we choose to reconstruct the Hubble diagram from SNe Ia data by employing the Gaussian process method.

The SNe Ia data used in this work is the Pantheon+ sample, which includes 1701 light curves of 1550 distinct SNe Ia from 18 different sky surveys, with a redshift range of $0.001 < z < 2.26$ [34]. In order to reduce systematics from peculiar velocities of nearby SNe Ia ($z < 0.01$) and eliminate degeneracies with Cepheid variable measurements, we reconstruct the Hubble diagram $\mu(z)$ using only SNe Ia in the redshift range $0.01 < z < 2.26$. The distance modulus is defined as

$$\mu_{\mathrm{SN}} = m_B - M, \tag{4}$$

where m_B is the corrected apparent magnitude of the SNe Ia, which is calculated using the SALT2 method [34–38], and M is the absolute magnitude. In this paper, the prior for the absolute magnitude of supernovae is set to the result calibrated by Cepheid variables as used by SH0ES, that is $M = -19.253 \pm 0.027$ [39].

The Gaussian process is a generalization of the Gaussian distribution over continuous variables, and it is a method for reconstructing functional relations between physical quantities without relying on specific functional forms [40]. If a univariate function $f(x)$ follows a Gaussian process, then $f(x)$ at any x satisfies a Gaussian distribution with mean $\mu(x)$ and variance $\mathrm{Var}(x)$, and the covariance between different x is $\mathrm{Cov}[f(x), f(x')] = k(x, x')$, then this Gaussian process can be represented as

$$f(x) \sim \mathbb{GP}(\mu(x), k(x, x')), \tag{5}$$

where the correlation function $k(x, x')$ is a kernel function.

The Gaussian process has also been widely applied in cosmology [41–46]. Here we use the open-source Python

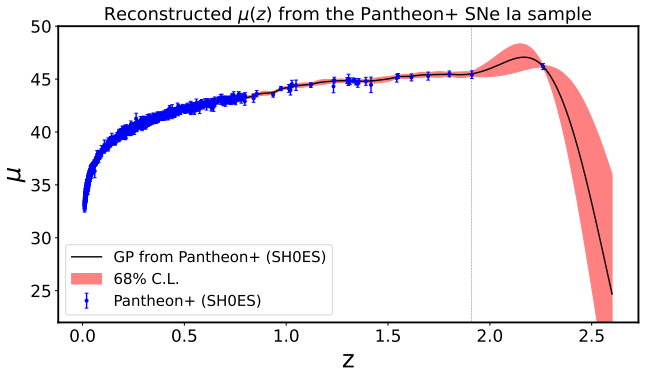

FIG. 1. Distance moduli $\mu(z)$ reconstructed via Gaussian process regression using the Pantheon+ SNe Ia sample. The absolute magnitude M adopts a Gaussian prior of $M = -19.253 \pm 0.027$ (i.e., SH0ES prior).

code `GaPP3` [41], which marginalizes the conditional probability distribution to obtain hyperparameters through the optimization algorithm, resulting in the distribution image of the predicted set. The reconstructed distance moduli $\mu(z)$ are shown in Fig. 1.

From Fig. 1, one can see that the oscillations become significantly larger beyond $z \sim 2$. Thus, we just use the reconstructed $\mu(z)$ to the 145 HIIGs located in the range of $z < 2$. In other words, the reconstruction result is just effective for the 145 HIIGs among the entire 181 ones.

As discussed in Mu *et al.* [47], the double squared exponential kernel function has various advantages in using the Gaussian process to reconstruct the distance modulus from the Pantheon+ sample. Its form is

$$k(x,\tilde{x}) = \sigma_{f1}^2 \exp\left[-\frac{(x-\tilde{x})^2}{2\ell_1^2}\right] + \sigma_{f2}^2 \exp\left[-\frac{(x-\tilde{x})^2}{2\ell_2^2}\right], \quad (6)$$

where the parameters (σ_{f1}, ℓ_1, σ_{f2}, ℓ_2) are referred to as hyperparameters. Clearly, the correlation strength parameters σ_{f1} and σ_{f2} dominate the scale of the covariance matrix of $f(x)$, while the correlation length parameters ℓ_1 and ℓ_2 dominate the correlation length between different x. The kernel function in Eq. (6), has maximum likelihood for the Pantheon+ sample calibrated by SH0ES. Therefore, we follow Mu *et al.* [47] and use this kernel function.

After reconstructing the distance moduli $\mu(z)$ through the Gaussian process, one can further calculate the luminosity $L(\mathrm{H}\beta)$ for each HIIG by using Eqs. (2) and (3). The uncertainty of luminosity is estimated with the following formula,

$$\epsilon_{\log L}^2 = \frac{4}{25}\epsilon_\mu^2 + \epsilon_{\log f}^2, \quad (7)$$

where ϵ_μ and $\epsilon_{\log f}$ are the errors of the distance modulus $\mu(z)$ and the logarithm of emission line fluxes $\log f$.

III. ANALYSIS AND RESULTS

A. Corrections to the scaling L–σ relation

The analysis of Cao and Ratra [29] shows that the L–σ relation for HIIGs is standardizable, however, there are significant differences between the slopes of the scaling L–σ relation (i.e., Eq. (1)) obtained from low-redshift and high-redshift subsamples, respectively. It suggests two possibilities: (i) the existence of the redshift evolution of the L–σ relation; and (ii) the requirement of non-linear term in the L–σ relation.

Based on the above mentioned possibilities, we propose three possible forms of corrections to the **classic scaling L–σ relation**, i.e., Eq. (1), which are labeled as **Correction I–III**.

- **Correction I: Adding an extra redshift-evolutionary term**

$$\log L(\mathrm{H}\beta) = \alpha + \beta \log \sigma + \gamma_1 \log(1+\gamma_2 z). \quad (8)$$

- **Correction II: Adding two logarithmic redshift-dependent coefficients**

$$\begin{aligned}\log L(\mathrm{H}\beta) =& [1+\gamma_1 \log(1+\frac{z}{1+z})]\alpha \\ &+ [1+\gamma_2 \log(1+\frac{z}{1+z})]\beta \log\sigma.\end{aligned} \quad (9)$$

- **Correction III: Adding two nonlinear redshift-dependent coefficients**

$$\log L(\mathrm{H}\beta) = (1+\frac{\gamma_1 z}{1+z})\alpha + (1+\frac{\gamma_2 z}{1+z})\beta\log\sigma. \quad (10)$$

B. Statistical analysis

In our analysis, the likelihood is constructed as

$$\mathcal{L} = \prod_{i=1}^{N} \frac{1}{\sqrt{2\pi}\epsilon_{\mathrm{tot,i}}} \times \exp\left[-\frac{(\log L_{\mathrm{th,i}} - \log L_{\mathrm{obs,i}})^2}{2\epsilon_{\mathrm{tot,i}}^2}\right], \quad (11)$$

where N is the number of data points, and the theoretical prediction of the luminosity $L_{\mathrm{th,i}}$ is obtained from a certain L–σ relation, where the four options for the L–σ relation are presented in Eqs. (1) and (8)–(10). For each HIIG, the observational value of the luminosity $L_{\mathrm{obs,i}}$ can be obtained from Eqs. (2) and (3) based on the $\mu(z)$ reconstructed through the Gaussian process; while for each GEHR, $L_{\mathrm{obs,i}}$ is obtained from Eq. (2) with the luminosity distance (d_L) obtained from the local distance ladder.

In addition, $\epsilon_{\mathrm{tot,i}}$ is the total uncertainty of $\log L_{\mathrm{i}}$, the expression of which depends on the form of L–σ relation. Specifically, in the case of choosing classic scaling form or **Correction I** for the L–σ relation, the total uncertainty ϵ_{tot} takes the following expression,

$$\epsilon_{\mathrm{tot}}^2 = \epsilon_{\log L}^2 + \beta^2 \epsilon_{\log\sigma}^2 + \epsilon_{\mathrm{int}}^2. \quad (12)$$

When choosing the **Correction II**, one obtains,

$$\epsilon_{\rm tot}^2 = \epsilon_{\log L}^2 + [1+\gamma_2 \log(1+\frac{z}{1+z})]^2 \beta^2 \epsilon_{\log\sigma}^2 + \epsilon_{\rm int}^2, \quad (13)$$

Correspondingly, in the scenario of **Correction III**, one has

$$\epsilon_{\rm tot}^2 = \epsilon_{\log L}^2 + (1+\frac{\gamma_2 z}{1+z})^2 \beta^2 \epsilon_{\log\sigma}^2 + \epsilon_{\rm int}^2. \quad (14)$$

Furthermore, in Eqs. (12)–(14), $\epsilon_{\log L}^2$ is calculated with Eq. (7), $\epsilon_{\log\sigma}$ is the uncertainty of the logarithm of emission line velocity dispersion σ, which is obtained from the actual observations, and $\epsilon_{\rm int}$ serves as a measure of the intrinsic dispersion in $\log L$.

Following Chen *et al.* [48], we compute the posterior probability distributions for the model parameters and the Bayesian evidence by using the Python open-source package `PyMultiNest` [49], which serves as an interface to the `MultiNest` algorithm [50] based on the Nested sampling [51]. The `GetDist` [52] is used to analyze the Monte Carlo samples, and then to plot the marginalized 1-D and 2-D posterior probability distributions for the parameters.

1. *Model comparison for the $L-\sigma$ relation*

Observational constraints for the L–σ relation parameters are summarized in the upper portion of Table I, where a joint sample with 36 GEHRs and 145 HIIGs[2] is employed, and four options for the L–σ relation, including the classic scaling form in Eq. (1) and the three correction forms in Eqs. (8)–(10), are taken into account, respectively.

As mentioned above, the posterior probability distributions for the model parameters are computed with the `PyMultiNest` code, and the mean values of the parameters together with their 68% confidence limits are listed in Table I.

To compare the three proposed correction forms of L–σ relation with the classic scaling one, we choose to use the Bayesian evidence as the judgment criterion [53, 54]. We calculate the natural logarithm of the Bayesian evidence ($\ln \mathrm{B_i}$) for each scenario, and the relative log-Bayesian evidence ($\ln \mathrm{B_{i0}} = \ln \mathrm{B_i} - \ln \mathrm{B_0}$), where $\ln \mathrm{B_0}$ denotes the log-Bayesian evidence for the classic scaling L–σ relation. According to the empirical rule of evaluating the strength of evidence, $|\ln \mathrm{B_{i0}}| \in (0, 1.0)$, $(1.0, 2.5)$, $(2.5, 5.0)$, and $(5.0, +\infty)$ correspond to inconclusive, weak, moderate, and strong evidence, respectively, and the model with smaller $|\ln \mathrm{B_i}|$ is preferred [54]. The Bayesian evidence for each scenario is computed with the `PyMultiNest` code, and the values of $\ln \mathrm{B_i}$ and $\ln \mathrm{B_{i0}}$ are listed in the last two columns of Table I.

In the scenario of **Correction I**, the 68% confidence intervals of correction-term coefficients include $(\gamma_1, \gamma_2) = (0, 0)$, which means the classic scaling $L-\sigma$ relation is still compatible, wherein $\ln \mathrm{B_{i0}} < 0$ and $2.5 < |\ln \mathrm{B_{i0}}| < 5.0$ indicate moderate evidence in favor of the classic scaling relation over **Correction I**. In the scenario of **Correction II**, the correction-term coefficients satisfy $\gamma_1 > 0$ and $\gamma_2 < 0$ in the 99% confidence intervals, wherein $\ln \mathrm{B_{i0}} > 0$ and $|\ln \mathrm{B_{i0}}| > 15.0$ imply a strong evidence to support the **Correction II**. In the scenario of **Correction III**, the correction-term coefficients γ_1 and γ_2 satisfy $\gamma_1 > 0$ and $\gamma_2 < 0$ in the 99% confidence intervals, wherein $\ln \mathrm{B_{i0}} > 0.0$ and $|\ln \mathrm{B_{i0}}| > 10.0$ imply a strong evidence to support the **Correction III**. Moreover, $|\ln \mathrm{B_{20}}| > |\ln \mathrm{B_{30}}|$ means that the **Correction II** is more competitive than the **Correction III**.

Overall, the **Correction II** is statistically favored, revealing clear evidence for redshift evolution in the L–σ relation. However, its performance remains imperfect, particularly for high-z HIIGs. This suggests the need for improved parameterizations of the relation—for instance, by incorporating additional properties like star-forming region size or metallicity [8]. Unfortunately, such observational data are scarce for most high-z HIIGs. We therefore propose to investigate alternative approaches in future work.

To conveniently compare the **Correction II** with the classic scaling form of L–σ relation, we display their precisions on fitting the data points in Fig. 2. In the upper panel, besides the data points, we also plot the classic scaling L–σ relation with (α, β) taking their mean values from Table I, and the **Correction II** with the redshift z taking five different values from 0 to 2.5 and the parameters $(\alpha, \beta, \gamma_1, \gamma_2)$ taking their mean values. Overall, the **Correction II** fits the data points much better in comparison to the classic scaling one.

The lower panel of Fig. 2 shows the residual distributions. We can see that the residual distribution of **Correction II** is almost identical to that of the classic scaling one in the lower-redshift range. However, for the higher-redshift HIIGs, the residual distribution for the **Correction II** is more concentrated around 0 than that for the classic scaling form. It means the redshift evolution terms of L–σ relation in the **Correction II** are necessary for the HIIGs in the high-z regime.

2. *Cosmological application*

Furthermore, we evaluate the constraining power of the HIIGs and GEHRs data on cosmological parameters. Specifically, we constrain the ΛCDM model using a joint sample of 36 GEHRs and all 181 HIIGs, adopting the **Correction II** L–σ relation, which has been demon-

[2] As discussed in Section II B, the reconstruction for distance moduli $\mu(z)$ from the Gaussian process is more credible in the range of $z < 2$, and this redshift range covers 145 HIIGs among the entire 181. Here we need to use the reconstructed $\mu(z)$ for the HIIGs, so only 145 HIIGs are used.

TABLE I. Observational constraints on $L-\sigma$ relation parameters with 68% confidence intervals

Distance estimation	$L-\sigma$ relation	α	β	γ_1	γ_2	$\epsilon_{\rm int}$	$\ln \mathrm{B_i}$	$\ln \mathrm{B_{i0}}$
Reconstructed with Gaussian process	Classic relation	34.14 ± 0.19	4.42 ± 0.13	...	...	0.29 ± 0.02	-73.71	0
	Correction I	34.09 ± 0.20	4.45 ± 0.14	0.04 ± 1.21	0.98 ± 1.44	0.29 ± 0.02	-76.61	-2.90
	Correction II	33.77 ± 0.20	4.66 ± 0.14	0.93 ± 0.11	-4.01 ± 0.47	0.26 ± 0.02	-57.69	16.02
	Correction III	33.77 ± 0.20	4.66 ± 0.14	0.31 ± 0.04	-1.34 ± 0.16	0.26 ± 0.02	-60.43	13.28
Derived in a ΛCDM framework	Classic relation	34.01 ± 0.20	4.54 ± 0.13	...	...	0.30 ± 0.02	-78.44	0
	Correction I	33.96 ± 0.21	4.58 ± 0.15	0.27 ± 1.23	1.02 ± 1.42	0.30 ± 0.02	-81.26	-2.82
	Correction II	33.61 ± 0.20	4.80 ± 0.14	0.96 ± 0.11	-4.02 ± 0.42	0.26 ± 0.02	-60.00	18.44
	Correction III	33.62 ± 0.20	4.80 ± 0.14	0.32 ± 0.04	-1.35 ± 0.15	0.26 ± 0.02	-63.31	15.13

[a]Observational constraints on the classic L–σ relation and three modified versions (**Corrections I-III**) from a combined sample of 36 GEHRs and 145 HIIGs. For each model, we report the log-Bayesian evidence ($\ln \mathrm{B_i}$) and relative evidence ($\ln \mathrm{B_{i0}} \equiv \ln \mathrm{B_i} - \ln \mathrm{B_0}$).

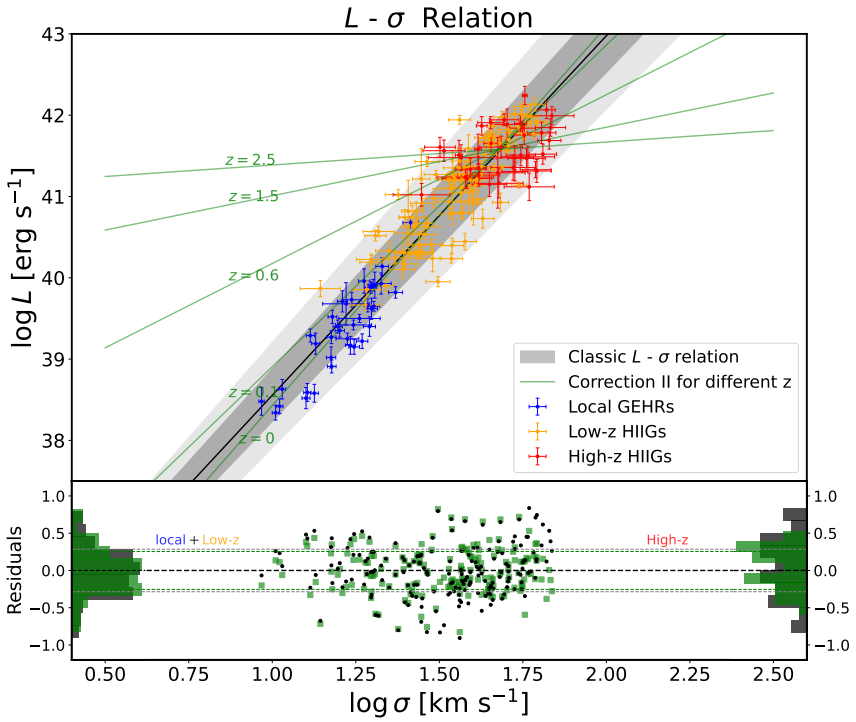

FIG. 2. Comparison of the classic L–σ relation (Eq. 1) and modified relation (**Correction II**; Eq. 9) fits to the combined sample of 36 GEHRs and 145 HIIGs. **Upper panel:** The black solid line shows the classical relation using mean parameter values (α, β) from Table I, with shaded 1σ regions. Green lines display **Correction II** for five redshift values (z = 0–2.5), using mean parameters (α, β, γ_1, γ_2). **Lower panel:** Residuals of $\log L(\mathrm{H}\beta)$ relative to both parameterizations (using mean parameters). Left histograms show local GEHRs and low-z HIIGs; right histograms show high-z HIIGs.

strated to be the most competitive among the four options considered.

To demonstrate the impact of the likelihood function's specific form on the results, we adopt the following three likelihood functions:

- **Full $\mathcal{L}$ with $\epsilon_{\rm int}$ = Const.**

  In this case, the likelihood function is expressed as Eq. (11), with the intrinsic dispersion $\epsilon_{\rm int}$ treated as a free parameter.

- **Full $\mathcal{L}$ with $\epsilon_{\rm int} = 0$**

  In this case, the likelihood function is given by Eq. (11), where the intrinsic dispersion $\epsilon_{\rm int}$ is fixed at zero.

- $\mathcal{L} \propto \exp(-\chi^2/2)$

In this case, the likelihood function is expressed as

$$\mathcal{L} \propto e^{-\chi^2/2}, \tag{15}$$

where χ^2 is

$$\chi^2 = \sum_{i=1}^{N} \frac{(\log L_{\rm th,i} - \log L_{\rm obs,i})^2}{2\epsilon^2_{\rm tot,i}}, \tag{16}$$

and N is the number of data points.

The marginalized 1-D and 2-D posterior probability distributions for the parameters of interest are shown in Fig. 3, while the mean values with 68% confidence limits for the parameters are listed in Table II.

We first focus on the constraints on the cosmological parameters, i.e., H_0 and Ω_m. The limits at 68% confidence level are $H_0 = 102.96 \pm 11.28$, 77.33 ± 4.19 and 70.95 ± 4.31[3] in the cases of taking full $\mathcal{L}$ with $\epsilon_{\rm int} =$ Const., full $\mathcal{L}$ with $\epsilon_{\rm int} = 0$ and $\mathcal{L} \propto \exp(-\chi^2/2)$, respectively; correspondingly, $\Omega_m = 0.50 \pm 0.26$, 0.43 ± 0.27 and 0.34 ± 0.28, respectively. According to the Planck 2018 results, the inferred values are $H_0 = 67.4 \pm 0.5$ and $\Omega_m = 0.315 \pm 0.007$ at 68% confidence level in the base-ΛCDM cosmology[55]. Only in the case of taking $\mathcal{L} \propto \exp(-\chi^2/2)$, the constraints on H_0 and Ω_m are consistent with those from the Planck 2018 results at 68% confidence level. While in the other two cases, the derived values of H_0 and Ω_m are significantly larger than those from the Planck 2018 results.

Then, we pay attention to the constraints on the parameters in the adopted L–σ relation, i.e., α, β, γ_1 and γ_2 in the **Correction II**. The limits at 68% confidence level are $(\alpha, \beta, \gamma_1, \gamma_2) = (34.46 \pm 0.27, 4.03 \pm 0.22, 0.52 \pm 0.10, -2.55 \pm 0.44)$ in the case of taking full $\mathcal{L}$ with $\epsilon_{\rm int} =$ Const., $(\alpha, \beta, \gamma_1, \gamma_2) = (33.57 \pm 0.14, 4.76 \pm 0.11, 0.18 \pm 0.07, -0.70 \pm 0.27)$ in the case of taking full $\mathcal{L}$ with $\epsilon_{\rm int} = 0$, and $(\alpha, \beta, \gamma_1, \gamma_2) = (33.27 \pm 0.16, 5.01 \pm 0.13, -0.09 \pm 0.10, 0.37 \pm 0.39)$ in the case of taking $\mathcal{L} \propto \exp(-\chi^2/2)$. In the first two cases, the parameter ranges of $\{\gamma_1, \gamma_2\}$ still exclude $\{0, 0\}$ at 95% confidence level. However, in the case of taking $\mathcal{L} \propto \exp(-\chi^2/2)$, the values $(\gamma_1, \gamma_2) = (0, 0)$ fall within the 68% confidence intervals. Such differences may arise from complex degeneracies among the parameters. As shown in Fig. 3, the observed parameter degeneracies include positive correlations in the $H_0 - \alpha$, $H_0 - \gamma_2$, $\alpha - \gamma_2$, and $\beta - \gamma_1$ planes, and negative correlations in the $H_0 - \beta$, $H_0 - \gamma_1$, $\alpha - \gamma_1$, $\beta - \gamma_2$, and $\gamma_1 - \gamma_2$ planes.

Overall, the constraints on H_0 and Ω_m from GEHRs + HIIGs are approximately an order of magnitude less precise than those derived from the Planck 2018 results. Moreover, the former agree with the latter at 68% confidence level only when adopting the likelihood function $\mathcal{L} \propto \exp(-\chi^2/2)$. Additionally, the specific form of the likelihood function significantly influences the inferred redshift evolution of the L-σ relation, possibly due to the complex degeneracies between cosmological parameters and the intrinsic parameters of the L-σ relation.

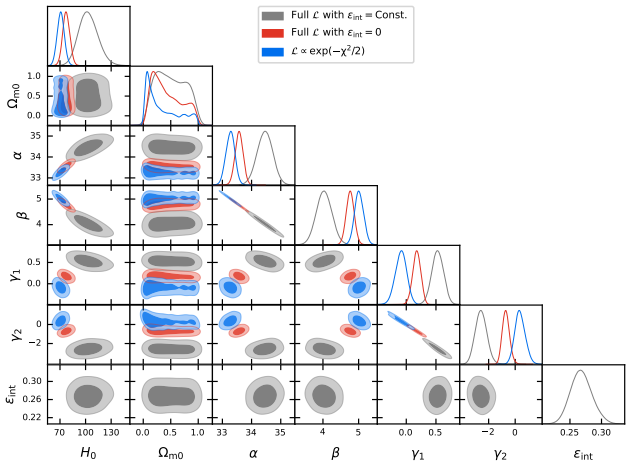

FIG. 3. Cosmological constraints in the ΛCDM framework using a combined sample of 36 GEHRs and 181 HIIGs. The analysis adopts **Correction II** for the L–σ relation and incorporates three distinct likelihood functions (see main text).

IV. DISCUSSIONS

As demonstrated by the posterior probability distributions of model parameters and Bayesian evidence values, the **Correction II** scenario emerges as the most competitive formulation for the L-σ relation. To validate the robustness of these primary findings, we must further examine whether the observed redshift evolution in the L-σ relation represents a genuine physical signal. Below, we assess this by investigating three key potential influencing factors: (1) SNe Ia absolute magnitude priors, (2) Malmquist bias effects, and (3) cosmological distance estimation methodologies.

A. Impact of Type Ia Supernova Absolute Magnitude Priors on Hubble Diagram Reconstruction

As discussed in Section II B, we must specify a prior on the absolute magnitude M of SNe Ia when using Gaussian process to reconstruct the Hubble diagram from SNe Ia data. While our baseline analysis adopts the SH0ES prior ($M = -19.253 \pm 0.027$), we also test an alternative prior from the Multicolor Light Curve Shape (MLCS) method ($M = -19.33 \pm 0.25$, Wang [56]).

The negligible impact on our key findings suggests that the results are not sensitive to the specific choice of M prior, reinforcing their robustness.

[3] H_0 has units of km s^{-1} Mpc^{-1}.

TABLE II. Constraints on both cosmological parameters and L–σ relation parameters with 68% confidence intervals

Likelihood function	H_0	Ω_{m0}	α	β	γ_1	γ_2	$\epsilon_{\rm int}$
Full $\mathcal{L}$ with $\epsilon_{\rm int} = $ Const.	102.96 ± 11.28	0.50 ± 0.26	34.46 ± 0.27	4.03 ± 0.22	0.52 ± 0.10	-2.55 ± 0.44	0.27 ± 0.02
Full $\mathcal{L}$ with $\epsilon_{\rm int} = 0$	77.33 ± 4.19	0.43 ± 0.27	33.57 ± 0.14	4.76 ± 0.11	0.18 ± 0.07	-0.70 ± 0.27	0.00
$\mathcal{L} \propto \exp(-\chi^2/2)$	70.89 ± 4.18	0.34 ± 0.29	33.27 ± 0.16	5.01 ± 0.13	-0.09 ± 0.10	0.37 ± 0.39	...

[a]Parameter constraints in the ΛCDM cosmology derived from a joint sample of 36 GEHRs and 181 HIIGs, using the modified L–σ relation (**Correction II**) and three distinct likelihood functions.

B. Impact of Malmquist Bias on the Redshift Evolution Significance in the $L-\sigma$ Relation

The observed high-redshift HIIGs are dominated by the most luminous systems due to selection effects, specifically Malmquist bias. To assess its impact, we compare fits from a high-z subsample ($z > 0.2$, $\log L > 41$) with those from a low-z subsample ($z < 0.2$, $\log L > 41$) under the classic L–σ relation. The resulting parameter tensions between the low-z and high-z subsamples reach 2.43σ (for α) and 2.50σ (for β). Without luminosity truncation in the low-z subset, these tensions increase to 5.59σ (for α) and 5.54σ (for β).

In summary, even after Malmquist bias correction, the redshift evolution in the L–σ relation persists, albeit with reduced significance.

C. Impact of Cosmological Distance Estimation Methods on the Redshift Evolution Significance in the $L-\sigma$ Relation

Within the baseline framework, we estimate cosmological distances using Gaussian process reconstruction of the Pantheon+ SNe Ia Hubble diagram. To evaluate the impact of distance estimation methods on our key results, we repeat the analysis under the flat ΛCDM model, adopting fiducial cosmological parameters from the Planck 2018 results ([55]). The corresponding constraints are presented in the lower section of Table I. Notably, the logarithmic redshift-dependent correction (**Correction II**) remains the most statistically favored.

These findings demonstrate that our primary conclusions are robust against variations in cosmological distance estimation methodologies.

V. SUMMARY

As the L-σ relation is fundamental for using HIIGs as standard candles, we have systematically investigated and compared four parameterizations of L-σ relation, including the classic scaling form and three redshift-dependent corrections. Using Gaussian process reconstruction of the Pantheon+ SNe Ia Hubble diagram to ensure cosmological model independence, we analyze a joint sample of GEHRs and HIIGs. The main results can be summarized as follows:

- The logarithmic redshift-dependent correction (**Correction II**) is strongly favored by Bayesian evidence ($|\ln B_{i0}| > 15$), with $\gamma_1 > 0$ and $\gamma_2 < 0$ excluded from zero at 99% confidence level. This correction significantly improves the fit for high-z HIIGs, reducing residuals by $\sim 30\%$ compared to the classic relation (Figure 2).

- The preference for **Correction II** persists when repeating the analysis in the ΛCDM model with adopting the Planck 2018 fiducial cosmological parameters (Table I), confirming its validity independent of distance estimation approaches.

- Our cosmological analysis in the flat ΛCDM framework, combining HIIGs and GEHRs, yields $H_0 = 70.89 \pm 4.18$ km s^{-1} Mpc^{-1} and $\Omega_m = 0.34 \pm 0.29$ (68% confidence level) under a χ^2-based likelihood. While consistent with Planck 2018 results, our constraints exhibit approximately an order-of-magnitude larger uncertainty (Table II). The strong parameter degeneracies between the $L-\sigma$ relation and cosmological parameters (Figure 3) demonstrate the necessity of combining multiple cosmological probes for robust parameter estimation.

While **Correction II** outperforms other forms, its residual dispersion at high-z suggests unaccounted physical drivers (e.g., metallicity or star-forming region size). Future observations of high-z HIIGs with ancillary data (e.g., JWST metallicity measurements) could further refine the L-σ relation and enhance its utility as a cosmological probe.

ACKNOWLEDGMENTS

We are grateful to Dr. Roberto Terlevich for helpful discussions on how to further examine whether the observed redshift evolution in the $L-\sigma$ relation represents a genuine physical phenomenon. This work has been supported by the National Key Research and Development Program of China (No. 2022YFA1602903), and the National Natural Science Foundation of China (Nos. 12588202, 12473002, 12075042 and 12475047).

[1] L. Searle and W. L. W. Sargent, Astrophys. J. **173**, 25 (1972).
[2] J. Bergeron, Astrophys. J. **211**, 62 (1977).
[3] R. Terlevich and J. Melnick, Mon. Not. Roy. Astron. Soc. **195**, 839 (1981).
[4] J. Melnick, M. Moles, R. Terlevich, and J.-M. Garcia-Pelayo, Mon. Not. Roy. Astron. Soc. **226**, 849 (1987).
[5] R. Terlevich *et al.*, Astron. Astrophys. Rev. Suppl. Ser. **91**, 285 (1991).
[6] D. Kunth and G. Östlin, Astron. Astrophys. Rev. **10**, 1 (2000), arXiv:astro-ph/9911094 [astro-ph].
[7] V. Bordalo and E. Telles, Astrophys. J. **735**, 52 (2011), arXiv:1104.4719 [astro-ph.CO].
[8] R. Chávez *et al.*, Mon. Not. Roy. Astron. Soc. **442**, 3565 (2014), arXiv:1405.4010 [astro-ph.GA].
[9] A. L. González-Morán *et al.*, Mon. Not. Roy. Astron. Soc. **505**, 1441 (2021), arXiv:2105.04025 [astro-ph.CO].
[10] J. Melnick, R. Terlevich, and M. Moles, Mon. Not. Roy. Astron. Soc. **235**, 297 (1988).
[11] E. R. Siegel *et al.*, Mon. Not. Roy. Astron. Soc. **356**, 1117 (2005), arXiv:astro-ph/0410612.
[12] M. Plionis *et al.*, Mon. Not. Roy. Astron. Soc. **416**, 2981 (2011), arXiv:1106.4558 [astro-ph.CO].
[13] R. Chavez *et al.*, Mon. Not. Roy. Astron. Soc. **425**, 56 (2012), arXiv:1203.6222 [astro-ph.CO].
[14] R. Terlevich *et al.*, Mon. Not. Roy. Astron. Soc. **451**, 3001 (2015), arXiv:1505.04376 [astro-ph.CO].
[15] D. Fernández Arenas *et al.*, Mon. Not. Roy. Astron. Soc. **474**, 1250 (2018), arXiv:1710.05951 [astro-ph.CO].
[16] A. L. González-Morán *et al.*, Mon. Not. Roy. Astron. Soc. **487**, 4669 (2019), arXiv:1906.02195 [astro-ph.GA].
[17] R. Chávez *et al.*, Mon. Not. Roy. Astron. Soc. **538**, 1264 (2025), arXiv:2404.16261 [astro-ph.CO].
[18] A. Sandage, in *Problems of Extra-Galactic Research*, Vol. 15, edited by G. C. McVittie (1962) p. 359.
[19] J. Melnick, Astrophys. J. **213**, 15 (1977).
[20] J. Melnick, Astron. Astrophys. **70**, 157 (1978).
[21] J. Kennicutt, R. C., Astrophys. J. **228**, 394 (1979).
[22] M. V. F. Copetti, M. G. Pastoriza, and H. A. Dottori, Astron. Astrophys. **156**, 111 (1986).
[23] J. Melnick, R. Terlevich, and E. Terlevich, Mon. Not. Roy. Astron. Soc. **311**, 629 (2000), arXiv:astro-ph/9908346 [astro-ph].
[24] K. Leaf and F. Melia, Mon. Not. Roy. Astron. Soc. **474**, 4507 (2018), arXiv:1711.10793 [astro-ph.CO].
[25] A. Hernández-Almada *et al.*, Mon. Not. Roy. Astron. Soc. **512**, 5122 (2022), arXiv:2112.04615 [astro-ph.CO].
[26] A. Mehrabi *et al.*, Mon. Not. Roy. Astron. Soc. **509**, 224 (2022), arXiv:2107.08820 [astro-ph.CO].
[27] S. Cao and B. Ratra, Phys. Rev. D **107**, 103521 (2023), arXiv:2302.14203 [astro-ph.CO].
[28] K. Ravi, A. Chatterjee, B. Jana, and A. Bandyopadhyay, Mon. Not. Roy. Astron. Soc. **527**, 7626 (2024), arXiv:2306.12585 [astro-ph.CO].
[29] S. Cao and B. Ratra, Phys. Rev. D **109**, 123527 (2024), arXiv:2310.15812 [astro-ph.CO].
[30] D. C. Koo *et al.*, Astrophys. J. Lett. **440**, L49 (1995).
[31] R. Guzman *et al.*, Astrophys. J. Lett. **460**, L5 (1996).
[32] Y. Wu *et al.*, Astrophys. J. **888**, 113 (2020), arXiv:1911.10959 [astro-ph.CO].
[33] H. Williams *et al.*, Astrophys. J. **969**, 54 (2024), arXiv:2309.16767 [astro-ph.GA].
[34] D. Brout *et al.*, Astrophys. J. **938**, 110 (2022), arXiv:2202.04077 [astro-ph.CO].
[35] M. Kunz, B. A. Bassett, and R. A. Hlozek, Phys. Rev. D **75**, 103508 (2007).
[36] J. Guy *et al.* (SNLS), Astron. Astrophys. **523**, A7 (2010), arXiv:1010.4743 [astro-ph.CO].
[37] R. Kessler and D. Scolnic, Astrophys. J. Lett. **836**, 56 (2017), arXiv:1610.04677 [astro-ph.CO].
[38] D. Brout *et al.*, Astrophys. J. **938**, 111 (2022), arXiv:2112.03864 [astro-ph.CO].
[39] A. G. Riess *et al.*, Astrophys. J. Lett. **934**, L7 (2022), arXiv:2112.04510 [astro-ph.CO].
[40] C. E. Rasmussen and C. K. I. Williams, *Gaussian Processes for Machine Learning* (The MIT Press, 2005).
[41] M. Seikel, C. Clarkson, and M. Smith, J. Cosmol. Astropart. Phys. **2012** (6), 036, arXiv:1204.2832 [astro-ph.CO].
[42] A. Shafieloo, A. G. Kim, and E. V. Linder, Phys. Rev. D **85**, 123530 (2012), arXiv:1204.2272 [astro-ph.CO].
[43] J. P. Hu and F. Y. Wang, Mon. Not. Roy. Astron. Soc. **517**, 576 (2022), arXiv:2203.13037 [astro-ph.CO].
[44] N. Liang, Z. Li, X. Xie, and P. Wu, Astrophys. J. **941**, 84 (2022), arXiv:2211.02473 [astro-ph.CO].
[45] J.-Z. Qi, P. Meng, J.-F. Zhang, and X. Zhang, Phys. Rev. D **108**, 063522 (2023), arXiv:2302.08889 [astro-ph.CO].
[46] T. Liu and K. Liao, Mon. Not. Roy. Astron. Soc. **528**, 1354 (2024), arXiv:2309.13608 [astro-ph.CO].
[47] Y. Mu, B. Chang, and L. Xu, J. Cosmol. Astropart. Phys. **2023** (9), 041, arXiv:2302.02559 [astro-ph.CO].
[48] Y. Chen, S. Kumar, B. Ratra, and T. Xu, Astrophys. J. Lett. **964**, L4 (2024), arXiv:2401.13187 [astro-ph.CO].
[49] J. Buchner *et al.*, Astron. Astrophys. **564**, A125 (2014), arXiv:1402.0004 [astro-ph.HE].
[50] F. Feroz, M. P. Hobson, and M. Bridges, Mon. Not. Roy. Astron. Soc. **398**, 1601 (2009).
[51] J. Skilling, AIP Conf. Proc. **735**, 395 (2004).
[52] A. Lewis, arXiv e-prints , arXiv:1910.13970 (2019), arXiv:1910.13970 [astro-ph.IM].
[53] R. E. Kass and A. E. Raftery, J. Am. Statist. Assoc. **90**, 773 (1995).
[54] R. Trotta, Contemp. Phys. **49**, 71 (2008), arXiv:0803.4089 [astro-ph].
[55] N. Aghanim *et al.* (Planck Collaboration), Astron. Astrophys. **641**, A6 (2020), arXiv:1807.06209 [astro-ph.CO].
[56] Y. Wang, Astrophys. J. **536**, 531 (2000), arXiv:astro-ph/9907405 [astro-ph].